Organic Electronics 13 (2012) 71–83

Contents lists available at SciVerse ScienceDirect

Organic Electronics

journal homepage: www.elsevier.com/locate/orgel

Control of electronic properties of triphenylene by substitution

A. Thiessen [a,1], H. Wettach [b], K. Meerholz [a], F. Neese [c], S. Höger [b], D. Hertel [a,*]

[a] Department für Chemie, Physikalische Chemie, Universität zu Köln, Luxemburgerstrasse 116, 50939 Köln, Germany
[b] Kekulé-Institut für Organische Chemie und Biochemie, Rheinische Friedrich-Wilhelms-Universität Bonn, Gerhard-Domagk-Strasse 1, 53121 Bonn, Germany
[c] Max-Planck-Institut für Bioanorganische Chemie, Stiftstrasse 34–36, 45470 Mülheim an der Ruhr, Germany

ARTICLE INFO

Article history:
Received 23 July 2011
Received in revised form 3 October 2011
Accepted 3 October 2011
Available online 19 October 2011

Keywords:
OLED
Phosphorescence
Singlet–triplet gap tuning
TD-DFT
Triphenylene

ABSTRACT

We report a joint theoretical and experimental study of the electronic properties of triphenylene based polycyclic aromatic hydrocarbons. Their aggregation tendency is suppressed by phenyl- or diphenylamino-substitution. The influence of the substituents on the absorption properties is investigated by time-dependent density functional theory (TD-DFT). Upon chemical modification of the triphenylene core, the singlet–triplet energy gap can be reduced by up to 0.4 eV. This prediction is spectroscopically verified. As a demonstration of the potential of these materials, Ir(III) doped phosphorescent organic light-emitting diodes (OLEDs) are tested, and limits of the performance are investigated. We achieve efficiencies above 30 Cd/A for simple, green-emitting two layer devices.

1. Introduction

Conjugated organic materials are promising candidates for applications in a variety of optoelectronic devices. In addition to the favourable mechanical properties, the electronic properties of organic molecules can be tailored by advanced synthetic methods. This has led to improved materials with high fluorescence quantum yields in the solid state [1] and high charge transporting capabilities [2] resulting in their utilization as active material in light-emitting diodes (OLEDs) [3], field-effect transistors [4], memory elements [5] or solar cells [6]. In the field of OLEDs a breakthrough was achieved by Forrest and coworkers who were the first to use phosphorescence in addition to fluorescence emission [7,8]. This, combined with doping technology, led to impressive improvements in device performance [9]. OLEDs are not only suitable to serve as active elements in displays, but also the application in solid state lighting is within reach [10]. So far, the best performance was realized with devices based on vacuum or gas-phase deposition processes [9,11,12] by careful optimization of device architectures and especially the combination of host and emitter materials. For commercial applications, however, solution processing might offer cost advantages over vacuum based technology. Conventionally, solution processing suffers from the difficulty of fabricating multi-layer devices due to the necessary use of orthogonal solvents. Crosslinkable materials can overcome this problem [13]. However, this approach is somewhat limited due to the additional steps in the material synthesis necessary for their screening for device applications.

Moreover, solution processed phosphorescent OLEDs are often fabricated by mixing multiple components to achieve optimized devices. For example, devices fabricated from polyvinylcarbazole (PVK) as host matrix and Ir(III) dyes as emitters contain additional electron transporting materials, e.g. oxadiazoles, to improve the charge balance. Upon the recognition of the importance of charge balance in solution processed phosphorescent devices [14], the performance of these types of OLEDs has been improving steadily, reaching the limit of quantum efficiency in the blue and green spectral range [15,16]. However, PVK degrades very fast, and only few other solution processed

* Corresponding author.
E-mail address: dirk.hertel@uni-koeln.de (D. Hertel).
[1] Present address: Nanoscale Optoelectronics Group, Department of Physics, University of Utah, Salt Lake City, USA.

1566-1199/$ - see front matter © 2011 Elsevier B.V. All rights reserved.
doi:10.1016/j.orgel.2011.10.005

matrix materials with equally good performance have been explored [17–19].

Some prerequisites for an host material are good electron and hole mobilities, formation of stable amorphous films, and high solubility. Further, the matrix has to be transparent, implying a wide gap between the highest occupied molecular orbital (HOMO) and lowest unoccupied molecular orbital (LUMO). However, the gap must not be too large, otherwise barriers for injection of electrons and holes due to a mismatch of electrode work functions and HOMO/LUMO levels are likely to reduce device performance. In addition, the gap of the triplet level of the host/guest has to be wide enough to prevent a back transfer of excitons from the emitting dopant to the matrix [20]. This necessitates a large HOMO/LUMO gap of the host, which is detrimental to charge injection in conventional materials, as described above. Reducing the singlet–triplet coupling would be one way to escape from this dilemma. However, apart from the influence of the conjugation length of organic [21,22] and metal organic [23] polymers on that gap, little is known with respect to the substituent influence on that issue.

Triphenylene possesses a wide gap and has favourable charge carrier mobilities [24,25] making it possible to abandon additional electron transport compounds that are known to be unstable. The high mobility is due to the rigid structure minimizing the deformation of the molecule in the charged state (low polaron binding energy) and an appreciable overlap of wavefunctions between neighbouring molecules [25]. However, the formation of excimers or exciplexes has to be prevented at the same time. Triphenylenes offer not only the advantage of easy purification but the easy accessibility of large quantities due to simple synthesis [26].

Recently, investigations of polymers containing triphenylene revealed a significant influence of substitution on the energy levels, revealing large reductions of the singlet–triplet gap from 0.7 to 17 meV [27]. Such a huge reduction is unusual. From experimental spectra alone it might be difficult to tell what the "real" singlet–triplet splitting is, since the singlet state might not be localised on the triphenylene in all polymers used in this study [27]. However, a detailed understanding of structure–property relations requires the combination of theoretical, syntheticaly and spectroscopic methods applied to carefully designed model compounds and the testing of their actual performance in a device. Such detailed investigations might also be beneficial for spintronic applications [28–30] and for harvesting triplets in solar cells in next generation devices [31] using upconversion of triplet to singlet states.

Here, we report a joint theoretical and experimental study of a series of triphenylene based polycyclic aromatic hydrocarbons as matrix materials for green-emitting phosphorescent OLEDs. We theoretically investigate the effect of substitution on the energy levels of triphenylene and compare the results to spectroscopic data. We found that appropriate substitution reduces the singlet–triplet gap of triphenylenes by about 0.4–0.3 eV. The performance of the new materials in OLEDs doped with $Ir(mppy)_3$ is tested, and the limits of the performance are investigated. During the course of our studies, we achieved efficiencies above 30 Cd/A for simple two layer devices.

2. Materials, methods and device preparation

THF was dried over Na and benzophenone, distilled and stored under Argon if necessary. Reagents were purchased at reagent grade from commercial sources and used without further purification. **TPTP** [32,33], **2** [34] and **5** [35] were prepared according to literature procedures (see Scheme 1 for structures and reactions). All air-sensitive reactions were carried out using standard Schlenk techniques under Argon. $P(tBu)_3$ was handled and transferred into the reaction flasks in a Glove-Box. Macherey–Nagel precoated TLC plates (Alugram® SIL G/UV_{254}, 0.2 mm) were used for thin-layer chromatography (TLC) analysis. Silica gel 60 M (Macherey–Nagel, 0.04–0.063 mm, 230–400 mesh) was used as the stationary phase for column chromatography. ^1H, ^{13}C and ^{19}F NMR spectra were recorded on Bruker DPX 300 (^1H, 300 MHz; ^{13}C, 75.5 MHz; ^{19}F, 282 MHz), DPX 400 (^1H, 400 MHz; ^{13}C, 101 MHz) and DPX 500 (^1H, 500 MHz; ^{13}C, 126 MHz; ^{19}F, 471 MHz) spectrometers, and chemical shifts are reported as δ values (ppm) and referenced to residual ^1H or ^{13}C signals in deuterated solvents. EI HRMS Mass spectra were measured on a Finnigan ThermoQuest MAT 95 XL, MALDI HRMS data were recorded on a Bruker Daltonics Apex IV FT-ICR and ESI HRMS data were recorded on a Bruker Daltonics ESI micrOTOF-Q instrument. Melting points were determined using a Leica DMLB microscope with hot stage and a home-built control unit. The values obtained were indicated without correction. Cyclic voltammetry was performed with a VA-Standard 663 and mAutoLab Type III Potentiostat (Metrohm, Switzerland) with a platinum disk as working electrode on diluted solutions of the respective compounds in dried and oxygen-free dichloromethane with 0.1 M tetrabutylammonium hexafluorophosphate (electrochemical grade, FLUKA) as supporting electrolyte, a graphite counter electrode, and a Ag/AgCl reference electrode Redox potentials were referenced against ferrocene/ferrocenium (Fc/Fc^+). The corresponding highest occupied molecular orbital (HOMO) and lowest unoccupied molecular orbital (LUMO) were calculated using the half wave potential of $E_{1/2}{}^{ox1}$ and $E_{1/2}{}^{red1}$ and using the absolute value of -5.1 eV to vacuum for the Fc/Fc^+ redox potential.

TPTP: A mixture of phencyclone (**1**, 2.0 g, 5.2 mmol) and diphenylacetylene (1.85 g, 10.4 mmol) in β-decalol (10 mL) was stirred at 250 °C for 3 h. The mixture was allowed to cool to RT, diluted with a minimum amount of dichloromethane and the product precipitated by the addition of methanol. After collection by filtration, the crude product was purified by column chromatography on silica gel using CH_2Cl_2/petrol ether (1:1) as eluent yielding **2** as colourless solid (1.34 g, 2.52 mmol, 48%) after subsequent precipitation from dichloromethane/methanol. ^1H NMR (300 MHz, $CDCl_3$): δ 8.44 (dd, 2 H, J = 1.1 Hz, J = 8.2 Hz), 7.63 (dd, 2 H, J = 0.9 Hz, J = 8.5 Hz), 7.42 (ddd, 2 H, J = 1.1 Hz, J = 7.1 Hz, J = 8.2 Hz), 7.14–7.08 (m, 10 H), 7.05 (ddd, 2 H, J = 1.3 Hz, J = 7.1 Hz, J = 8.4 Hz), 6.96–6.89 (m, 6 H), 6.76–6.71 (m, 4 H); ^{13}C NMR ($CDCl_3$, 100 MHz): δ 142.8, 140.3,

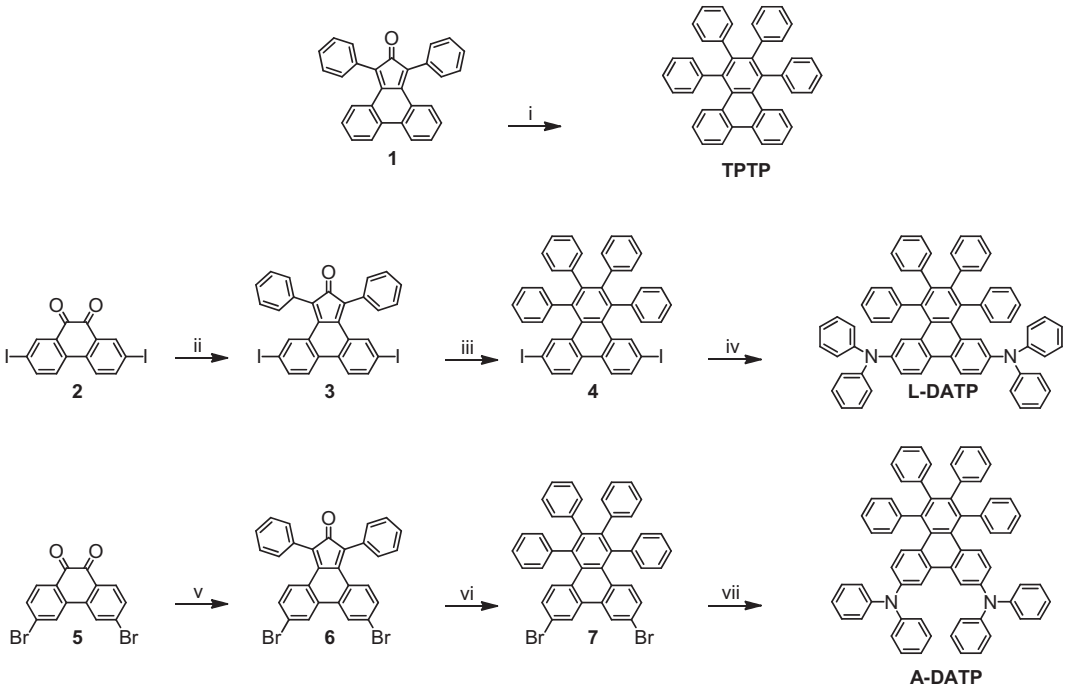

Scheme 1. Structures and synthesis of the investigated triphenylenes.

140.3, 137.1, 132.0, 131.5, 131.5, 131.1, 130.7, 129.9, 127.9, 126.5, 126.3, 126.1, 125.4, 125.1, 123.1; EI MS *m*/*z* (M^+) calc. for $C_{42}H_{28}$: 532.2; found 532.2.

Compound **3**: A mixture of **2** [34] (2.5 g, 5.4 mmol) and 1,3-diphenylacetone (1.2 g, 5.7 mmol) in methanol (50 mL) was stirred at reflux temperature and NaOH (0.50 g, 8.9 mmol) in methanol (8 mL) was slowly added dropwise. The mixture was heated at reflux temperature for one additional hour, cooled to RT, the precipitated solid was collected by filtration (2.64 g, 4.16 mmol, 77%) and used for the next step without purification. Due to its hard solubility, only a mass spectrum could be obtained for its characterization. EI *m*/*z* (M^+) calc. for $C_{29}H_{16}I_2O$: 633.9; found 633.9.

Compound **4**: A mixture of **3** (271 mg, 0.43 mmol) and diphenylacetylene (360 mg, 1.72 mmol) in β-decalol (1 mL) was stirred at 250 °C for 2 h. The mixture was allowed to cool to RT, diluted with a minimum amount of dichloromethane and the product precipitated by the addition of methanol. After collection by filtration, the crude product was purified by column chromatography on silica gel using CH_2Cl_2/petrol ether (1:5) as eluent yielding **4** as yellow solid (157 mg, 0.2 mmol, 13%) after subsequent precipitation from dichloromethane/methanol. ^{1}H NMR (300 MHz, *CDCl*$_3$): δ 8.06 (d, 2 H, J = 8.6 Hz), 7.89 (d, 2 H, J = 1.8 Hz), 7.66 (dd, 2 H, J = 1.7 Hz, J = 8.6 Hz), 7.21–7.14 (m, 6 H), 7.07–7.03 (m, 4 H), 6.95–6.87 (m, 6 H), 6.72–6.68 (m, 4 H); ^{13}C NMR ($CDCl_3$, 100 MHz): δ 141.8, 141.1, 139.8, 139.3, 137.4, 135.0, 132.3, 131.7, 131.3, 130.0, 130.0, 128.2, 126.7, 126.6, 125.4, 124.3, 91.7; EI MS *m*/*z* (M^+) calc. for $C_{42}H_{26}I_2$: 784.0; found: 783.9.

L-DATP: Toluene (4.5 mL) was added to a mixture of **4** (182 mg, 0.23 mmol), diphenylamine (86 mg, 0.51 mmol), $Pd_2(dba)_3$ (11 mg, 0.012 mmol), NaOtBu (66 mg, 0.7 mmol) and ($P(tBu)_3$ (3 mg, 0.014 mmol) and the solution was stirred at 80 °C for 16 h. The mixture was allowed to cool to RT, and diluted with water and diethylether. The organic phase was washed with water, $NaHCO_3$ solution and brine, and dried over $MgSO_4$. After removing the solvent, the crude product was purified by column chromatography on silica gel using CH_2Cl_2/petrol ether (2:5) as eluent yielding **L-DATP** as a slightly yellow solid (120 mg, 0.14 mmol, 60%) after subsequent precipitation from dichloromethane/methanol. ^{1}H NMR (300 MHz, $CDCl_3$): δ 8.18 (d, 2 H, J = 8.8 Hz), 7.20 (d, 2 H, J = 2.2 Hz), 7.08–7.00 (m, 10 H), 6.85–6.80 (m, 4 H), 6.73–6.63 (m, 24 H), 6.53–6.48 (m, 4 H); ^{13}C NMR (CD_2Cl_2, 125 MHz): δ 132.5, 132.4, 130.2, 129.1, 127.5, 127.1, 126.7, 126.2, 125.6, 125.1, 124.9, 123.5; EI MS *m*/*z* (M^+) calc. for $C_{66}H_{46}N_2$ 866.4; found: 866.2.

Compound **6**: A mixture of **5** [35] (3.47 g, 9.48 mmol) and 1,3-diphenylacetone (2.09 g, 9.95 mmol) in methanol (50 mL) was stirred at reflux temperature and KOH (0.885 g, 15.24 mmol) in methanol (10 mL) was slowly added dropwise. The mixture was heated at reflux temperature for additional 30 min, then cooled to 0 °C, and the precipitated solid was collected by filtration (4.09 g, 7.57 mmol, 80%) and used for the next step without purification. Due to its hard solubility, only a mass spectrum could be obtained for its characterization. EI *m*/*z* (M^+) calc. for $C_{29}H_{16}Br_2O$: 540.2; found 540.2.

Compound **7**: A mixture of **6** (1.00 g, 1.85 mmol) and diphenylacetylene (394 mg, 2.22 mmol) in β-decalol (6 mL) was stirred at 250 °C for 20 h. The mixture was allowed to cool to RT, diluted with chlorobenzene and the product precipitated by the addition of methanol. After

collection by filtration, the crude product was purified by column chromatography on silica gel using CH_2Cl_2/petrol ether (1:2) as eluent yielding **2** as yellow solid (124 mg, 0.18 mmol, 10%) after subsequent precipitation from dichloromethane/methanol. ^{1}H NMR (300 MHz, $CDCl_3$): δ 8.50 (d, 2 H, J = 2.1 Hz), 7.43 (d, 2 H, J = 9.0 Hz), 7.16–7.00 (m, 12 H), 6.94–9.85 (m, 6 H), 6.75–6.69 (m, 4 H); ^{13}C NMR (CD_2Cl_2, 100 MHz): δ 142.6, 141.4, 140.4, 137.6, 132.4, 132.2, 131.8, 131.7, 130.7, 130.3, 129.2, 128.4, 126.9, 126.8, 126.2, 125.7, 121.1; EI MS m/z (M^+) calc. for $C_{42}H_{26}Br_2$: 690.0; found: 690.1.

A-DATP: Toluene (4 mL) was added to a mixture of **7** (124 mg, 0.18 mmol), diphenylamine (67 mg, 0.40 mmol), $Pd_2(dba)_3$ (9 mg, 0.009 mmol), NaOtBu (52 mg, 0.45 mmol) and ($P(tBu)_3$ (2.5 mg, 0.01 mmol) and the solution was stirred at 80 °C for 24 h. The mixture was allowed to cool to RT, and diluted with water and diethylether. The organic phase was washed with water, $NaHCO_3$ solution and brine, and dried over $MgSO_4$. After removing the solvent, the crude product was purified by column chromatography on silica gel using CH_2Cl_2/petrol ether (1:2) as eluent yielding **A-DATP** as a slightly yellow solid (104 mg, 0.12 mmol, 67%) after subsequent precipitation from dichloromethane/methanol. ^{1}H NMR (300 MHz, $CDCl_3$): δ 7.58 (d, 2 H, J = 2.5 Hz), 7.34 (d, 2 H, J = 9.2 Hz), 7.20–7.16 (m, 8 H), 7.09–7.03 (m, 18 H), 7.02–6.97 (m, 4 H), 6.89–6.84 (m, 6 H), 6.72–6.66 (m, 6 H); ^{13}C NMR ($CDCl_3$, 125 MHz): δ 131.8, 131.4, 130.4, 129.0, 127.7, 126.3, 125.9, 124.9, 124.6, 123.1, 120.4, 115.8; EI MS m/z (M^+) calc. for $C_{66}H_{46}N_2$: 866.4; found: 866.4.

2.1. Theoretical methods

Calculations were carried out with the ORCA program system (version 2.6.03). The structure of **TPTP** was initially built graphically and optimized with the semi-empirical AM1 method. The resulting minimum energy structure was subjected to an energy minimization using the BP86 functional [36,37] and the SV(P) [38] basis set.

The structure of **L-DATP** was derived from **TPTP** by replacing hydrogens on the appropriate rings with N(phenyl)$_2$ substituents followed by energy minimization at the BP/SV(P) level of theory. Isomer **A-DATP** was derived from **L-DATP** by manually moving the N(phenyl)$_2$ substituents followed by complete re-optimization. The energy of **A-DATP** was found to be slightly ($\sim$3 kcal/mol) lower than that of **L-DATP**. Two rounds of optimization were carried out. The first set of structures was obtained from standard BP86/SV(P) calculations and the second set of structures included additionally empirical van der Waals corrections from Grimme [39]. Electronic transitions were calculated using TD-DFT [40]. In order to minimize chances to miss the lowest excited states, five singlet and five triplet roots were calculated. Since TD-DFT is sometimes plagued by artefacts concerning charge transfer states [41], we have calculated the electronic transitions at several levels of theory. From preliminary calculations, the best results were obtained with the B3LYP functional [42], which was therefore employed for the computations.

2.2. Electro-optical methods

Photoluminescence spectra of the compounds were measured on liquid or solid solutions of the respective compound in cyclohexane, tetrahydrofurane, toluene or dichloromethane (DCM), as well as on pure, thin, spin coated films or on drop casted films of the compounds in polystyrene. All samples were prepared in a nitrogen-filled glove box excluding oxygen.

2.2.1. Fluorescence quantum yield measurements

The quantum yields of the films were obtained using a quantum yield measurement system (Hamamatsu C9000) using 340 nm light for excitation. The equipment is operated in a nitrogen glove box to exclude oxygen.

2.2.2. Time-resolved photoluminescence

Time resolved fluorescence of the triphenylene derivatives was measured with a MINI-TAU spectrometer from Edinburgh Instruments with a diode laser (375 nm) as excitation source. The instrument response is approximately 100 ps.

2.2.3. Phosphorescence measurements

The setup is similar to a previously described system [43]. In short, the compounds were excited with the third harmonic (355 nm) of a Nd:YAG (Spitlight, Innolas) or the up-converted output (300 nm) of an OPO (GWU, versaScan) working at 600 nm. The laser operated at a repetition rate of 10 Hz. The PL was collected and focused onto the entrance slit of the monochromator and detected by an intensified gateable ICCD camera (Roper Scientific). The spectral resolution was set to 2 nm. The instrument response function achievable is about 1.7 ns (using stray-light detection). Time resolved measurements were performed at 295 and 80 K under a continuous flow of nitrogen.

For time resolved phosphorescence measurements the equipment was modified to provide stable operation of the laser, OPO/SHG and triggering of the ICCD at very low frequency down to 0.2 Hz.

2.2.4. OLED fabrication

Ir(mppy)$_3$ (tris(2-(4-tolyl)phenylpyridine)iridium) was purchased from American Dye Source. In some experiments the red emitter Ir(t-piq)$_2$(acac) (*bis*(1-(4-*tert*-butylphenyl) isoquinoline) Ir(III) acetylacetonate) and electron transport material OXD-7 (1,3-*bis*(5-(4-*tert*-butylphenyl)-1,3,4-oxadiazol-2-yl)benzene) from Sensient (Wolfen) were used. OLEDs were prepared on pre-cleaned, UV-ozone-treated ITO-coated glass substrates. A layer of 25 nm PEDOT:PSS (Clevios, Heraeus) was spin-coated onto the substrates under clean-room conditions, and baked at 150 °C for 10 min in a nitrogen glovebox to remove residual water.

The architecture of the devices is depicted in Scheme 2. The emission layer (EML) was fabricated from the dopant and matrix. The Ir(III) emitters were mixed with the matrix in toluene solution and spin-coated yielding layers of 80 nm (**A**), 60 nm (**B**) and 50 nm (**C**) thickness. For investigations of the electron transport, OXD-7 (25% by weight) was admixed to the solution. For comparison, OLEDs with the red Ir(III)

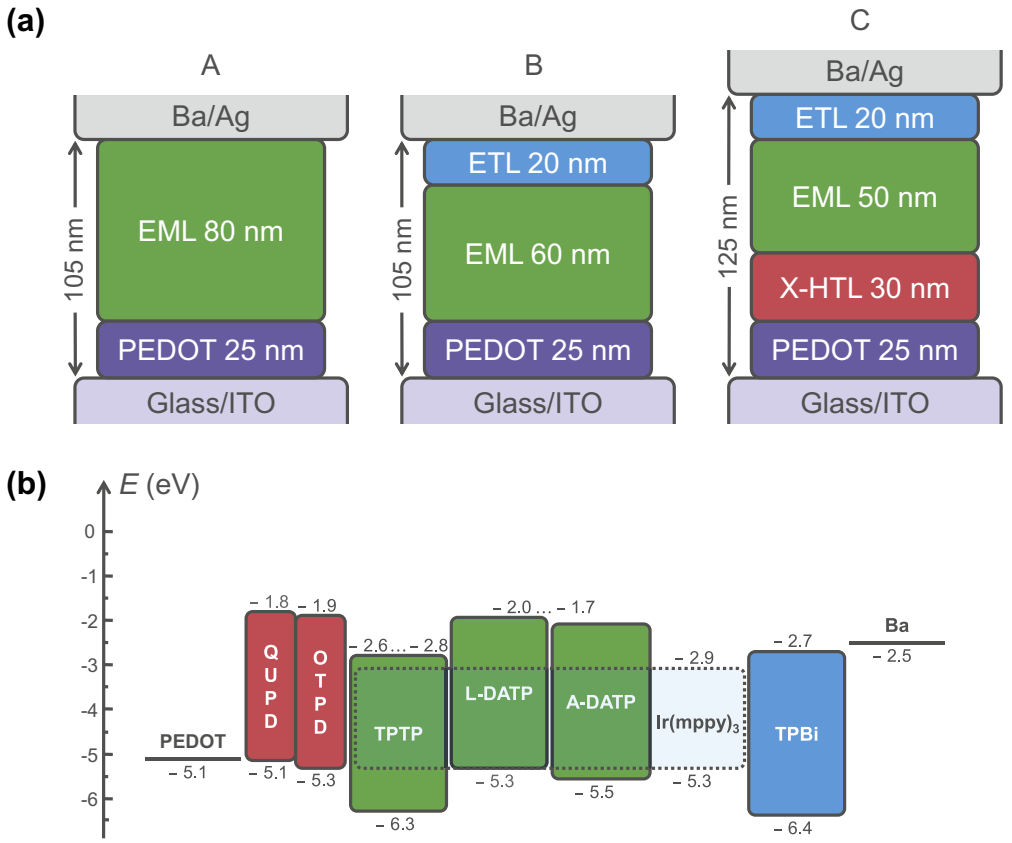

Scheme 2. The different device architectures (a) used for OLED testing and a sketch of the energy levels of investigated compounds (b).

emitter Ir(t-piq)$_2$(acac) were made. In some devices (**B** and **C**) a 20 nm thick layer of TPBi (1,3,5-Tris(1-phenyl-1H-benzo[d]imidazol-2-yl)benzol) was evaporated on top of the emitting layer with a rate of 0.5 nm/s at a base pressure of 10^{-6} mbar in a K.J. Lesker Spectros evaporation system. In devices of type **C** hole transporting layers QUPD and OTPD were prepared as described in literature [44] resulting in 20 nm and 10 nm thick films, respectively. The cathode consisting of Ba (4 nm) and Ag (100 nm) was deposited by thermal evaporation at a base pressure of 10^{-6} mbar. The current–voltage-luminescence characteristics were measured with a source-measure unit (Keithley 2400) and a calibrated photodiode under argon atmosphere. The EL spectra were measured with a fibre-coupled calibrated CCD spectrometer (Ocean Optics) in argon atmosphere.

3. Results and discussion

3.1. Synthesis

The synthesis of the phenyl-substituted triphenylenes is based on the Diels–Alder reaction between the corresponding phencyclones with diphenylacetylene and subsequent *in situ* decarbonylation under generation of an aromatic sextet structure. The basic structural motive, **TPTP** has already been described by Dilthey more than 70 years ago [32]. However, modern Pd-catalyzed amination methods allow the easy preparation of the corresponding diphenylamine substituted derivatives by starting from the diiodo or dibromo phenanthrenedionenes, respectively. Although the halogenated phencyclones could not be characterized in detail due to their low solubility, all subsequent intermediates were well soluble and could be easily isolated and purified. While **TPTP** is a colourless solid, the aminosubstituted derivatives **L-DATP** and **A-DATP** are slightly yellow, that were not described in literature before.

3.2. Theoretical modelling and spectroscopy

Optimized structures of **TPTP**, **A-DATP** and **L-DATP** are shown in Fig. 1. It is apparent that the triphenylene unit is distorted from a planar geometry, even in the **TPTP**. The calculations are able to predict the oscillator strength of the optical transitions at least qualitatively. **TPTP**'s S_1 state at around 3.70 eV (335 nm) has only low oscillator strength $f_{osc} \sim 0.002$ (Table 1, calculated energies refer to vertical transitions).

The oscillator strength for the transition from the ground state to the S_1 state increases upon substitution of hydrogen atoms with triphenylamines at the triphenylene core. In **A-DATP** the S_1 transition is predicted to be at 3.04 eV (408 nm) and at 2.96 eV (419 nm) in **L-DATP**, respectively. All investigated lowest excited states

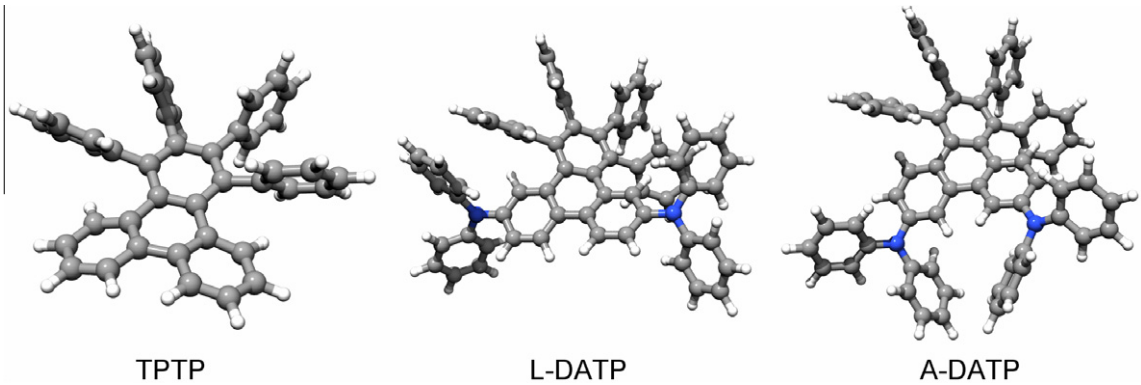

Fig. 1. Optimized ground state geometry of **TPTP**, **L-DATP** and **A-DATP**.

correspond to π–π transitions. The transition to S_2 of **L-DATP** and **A-DATP** is predicted to be at 3.02 eV (411 nm) and 3.14 eV (395 nm), respectively. Additionally, the oscillator strength of the S_2 transition of **L-DATP** and **A-DATP** increases compared with **TPTP** from $f_{osc} < 0.1$ to $f_{osc} \sim 0.1$ and $f_{osc} \sim 0.2$, respectively. The change in energy is partially due to the shift of electron density from the amine substituents to the triphenylene core upon excitation. This effect is illustrated in Fig. 2 where the calculated differential densities upon excitation for **TPTP**, **A-DATP** and **L-DATP** are plotted. A larger contribution to the change of transition energy and, additionally, to higher oscillator strength is due to the increase of the conjugated system.

In order to compare theoretical results in detail to experimental data of solid films we shortly discuss the effect of the surrounding medium on the energy of the optical transitions. One has to keep in mind that reorganization energies and solid state shifts or solvent shifts of the excited state energies are not accounted for in calculations. It is known that both contributions can amount to few tenth of an eV [45]. Thus, firstly we show exemplary the influence of solvent polarity on fluorescence and phosphorescence of **TPTP** and **L-DATP**. The solvents used are cyclohexane as unpolar and dichloromethane (DCM) as a polar solvent, respectively. The polarity of both compounds is 31 and 40 kcal/mol on the well-known empirical ET_{30} scale [46]. We used toluene as well, however its polarity (34 kcal/mol) is intermediate between cyclohexane and DCM, the results are between both and thus are not further discussed since they contain no new information.

The shape and position of absorption spectra of **TPTP** and **L-DATP** are independent on solvent polarity (Fig. 3,

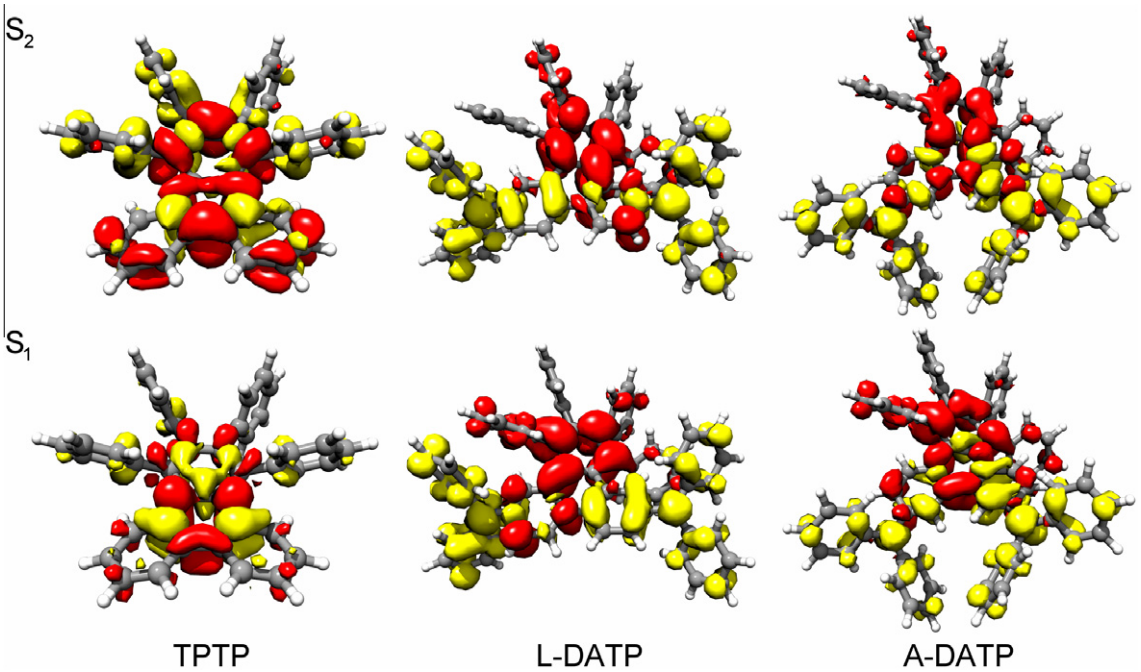

Fig. 2. Representation of the charge transfer upon excitation to the second (top row) and first (bottom row) excited singlet state of **TPTP**, **L-DATP** and **A-DATP**. The excited state electron density gain and loss are depicted in red and yellow, respectively. The first two excited states of **L-DATP** and **A-DATP** show a charge transfer shift to the triphenylene core associated with the amine substituents. (For interpretation of the references to colour in this figure legend, the reader is referred to the web version of this article.)

Table 2). The absorption of **TPTP** starts at 363 nm (3.42 eV) with a shoulder at 314 nm (3.95 eV) and its absorption maximum is at 288 nm (4.3 eV). As expected from calculations the absorption of **L-DATP** is red-shifted with respect to **TPTP**. The onset of absorption of **L-DATP** is located at 436 nm (2.84 eV). **L-DATP** has two pronounced absorption bands at 365 nm (3.4 eV) and at 292 nm (4.24 eV).

The energetic position and shape of fluorescence of **TPTP** is largely independent on solvent polarity (Fig. 3 and Table 2), thus pointing to a small influence of the polarizability of the surrounding medium on the excited state relaxation. This is different for **L-DATP** (Fig. 3 and Table 2). The peak of fluorescence of **L-DATP** in DCM is red-shifted by about 30 nm (160 meV) to 479 nm compared with the PL maximum in cyclohexane (451 nm). This is a consequence of the larger π-system and an increased dipole moment upon substitution with diphenylamine.

Upon photoexcitation of frozen (80 K) **TPTP** or **L-DATP** solutions (Fig. 3) a new, long-lived emission band appears in the green to red spectral region. We assign this emission to phosphorescence due to (i) its very low intensity, (ii) its absence at room temperature, (iii) its similar vibronic splitting compared with low temperature fluorescence spectra and, (iv) its lifetime of about 1 s (Table 2 and Fig. 4). Such a long phosphorescence lifetime has been observed in conjugated oligomers of polyphenylenes as well [47]. Additionally, the shape of emission spectra and the lifetime is independent of concentration in the range of 10^{-6}–10^{-4} mol/L. The energetic position of the phosphorescence spectrum of **TPTP** and **L-DATP** is only slightly dependent on solvent polarity. The total shift is less than 50 meV. Altogether the influence of polarity and polarizability of the surrounding medium on the exited state energy of **TPTP** and **L-DATP** is much less than 200 meV.

Now we discuss the results for the materials present in the form of solid films since it is more relevant for device applications and we compare them with theoretical calculations in detail.

Comparison of the predicted transition energies and oscillator strength with the measured absorption spectra shows reasonable agreement (Table 3). The predicted S_1 transition for **TPTP** (335 nm) compares well with the onset of absorption (~330 nm, Fig. 5). Taking into account the above discussed uncertainties for **A-DATP** and **L-DATP** the agreement with theory is fair. The predicted red-shift of the onset of absorption in both compounds compared with **TPTP**, however, is clearly visible (Fig. 5). For transitions at higher energy the oscillator strength increases as predicted. The assignment of definite transitions/energies is difficult due to inhomogeneously broadened absorption bands resulting from polarization effects of the disordered medium and the overlap with vibronic transitions. Comparison with the solution spectra bears out the same trends i.e. a red-shift and an increase in oscillator strength upon substitution of **TPTP**, no matter if the absorption edge or band maxima (or features visible as a shoulder in absorption bands) are identified with the transition energy.

As mentioned in the introduction aromatic hydrocarbons are often prone to aggregation which is often detrimental for some applications in optoelectronic devices. Triphenylene itself shows structured fluorescence spectra with well-resolved vibronic progression [48]. The featureless absorption of **TPTP**, **L-DATP** and **A-DATP** (Fig. 5) indicates a distorted geometry (Fig. 1) which is optimal for suppression of aggregation. The absence of aggregates is corroborated by the RT fluorescence spectra of the compounds in the solid state (Fig. 5). The emission is broad and featureless as in solution (Fig. 5). This is due to the

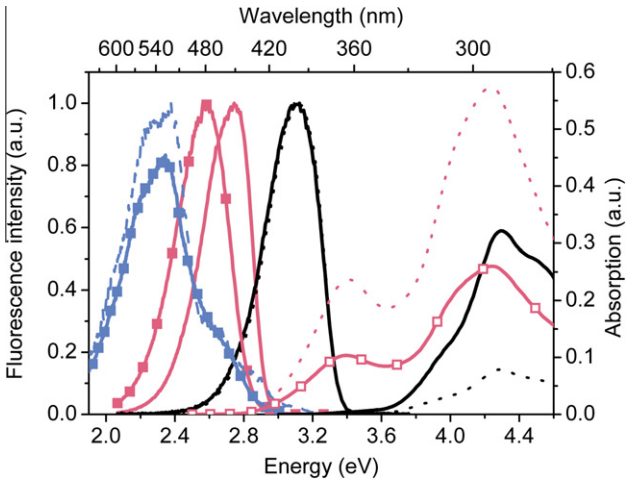

Fig. 3. Left axis: Fluorescence and phosphorescence spectra of solutions of **TPTP** and **L-DATP**. Fluorescence: **TPTP** (DCM, $c = 3.8 \times 10^{-6}$ mol/L, black solid line), **TPTP** (cyclohexane, $c \sim 1 \cdot 10^{-6}$ mol/L, black dotted line), **L-DATP** (cyclohexane, $c \sim 1 \times 10^{-4}$ mol/L, red solid line) and **L-DATP** (DCM, $c = 2.3 \times 10^{-6}$ mol/L, red solid line with solid squares). Phosphorescence (80 K): **L-DATP** (cyclohexane $c \sim 1 \times 10^{-4}$ mol/L, dashed blue line) and **L-DATP** (DCM, $c = 2.3 \times 10^{-6}$ mol/L, dashed blue line with squares). Right axis: Absorption spectra of **TPTP** and **L-DATP** solutions. **TPTP** (DCM, $c = 3.8 \times 10^{-6}$ mol/L, black solid line), **TPTP** (cyclohexane, $c \sim 1 \times 10^{-6}$ mol/L, black dotted line) **L-DATP** (cyclohexane, $c \sim 1 \times 10^{-5}$ mol/L, red dotted line) and **L-DATP** (DCM, $c = 2.3 \times 10^{-6}$ mol/L, red solid line with open squares). (For interpretation of the references to colour in this figure legend, the reader is referred to the web version of this article.)

disordered nature of the material allowing a high number of conformations by varying orientations for the aromatic substituents around a single bond. This leads to a variety of excited and ground state configurations inducing unstructured and broad emission and absorption spectra [49]. The weak change in position and shape of the spectra in going from solution to solid state further supports the view that the broad spectra are not a consequence of aggregation or excimer formation. This is supported by the absence of a concentration dependence of the emission spectra.

3.3. Estimation of the singlet–triplet gap

Of special interest in the present discussion is the singlet–triplet gap between the S_1 and the T_1 level. For OLEDs a higher T_1 level of the host relative to the T_1 level of the guest is beneficial, since it suppresses back-transfer from the T_1 of the guest to the host. Taking $Ir(mppy)_3$ as guest with a T_1 energy of roughly 2.4 eV the T_1 of the host has to be at 2.6 eV at minimum. In conventional aromatic hydrocarbons this would imply a S_1 level at 3.5 eV and a HOMO–LUMO gap in the UV with the consequence of large injection barriers for electrons and holes from the electrodes. Thus, high device efficiency is rather difficult to achieve.

The calculated splitting between the singlet excited state and the first triplet excited state (ΔE_{ST}) is given in Table 1. Apparently, substitution effectively reduces the energy gap, leading to a localisation of the triplet exciton on the triarylamine moieties. Comparison with experimental values bears out good agreement (Table 3). The values for the S_1 and T_1 energies of **A-DATP** and **L-DATP** have been obtained from the high energy peak of the fluorescence and phosphorescence spectra, respectively (80 K, Fig. 6)[50]. ΔE_{ST} is estimated to be 0.36 and 0.62 eV for **L-DATP** and **A-DATP**, respectively. Using DCM solution data (Table 2) the gap in **L-DATP** is 0.25 eV and thus even smaller. Comparison with the values derived from **TPTP** (and **L-DATP**) solutions supports our view that uncertainties due to polarization effects and poorly structured spectra of **TPTP** are small. The dielectric properties of the film seem to be comparable to the unpolar solvent cyclohexane since the energetic position of fluorescence and phosphorescence spectra are similar in cyclohexane solution and film.

To identify the S_1 transition energy of **TPTP** we used the shoulder on the high energy side of the thin film spectrum (Table 1, Fig. 6), since the energy of S_1 (400 nm) is close to the $S_0 \leftarrow S_1$ (0-0) transition of **TPTP** solutions (Fig. 3, Table 2). The S_1 energy is similar to related triphenylene compounds [27]. The singlet–triplet gap of **TPTP** amounts to 0.73 eV for solid film (or 0.8 eV for solution). The agreement of ΔE_{ST} calculations and the red-shifted spectra of **A-DATP** and **L-DATP** support our assignment to phosphorescence. Additionally, the identical vibronic splitting of fluorescence and phosphorescence is characteristic of originating from the same molecule/part of molecule (Fig. 6). This indicates that the localization of the excitations occurs partly in the substituents (compare with calculated differential densities of Fig. 2), in line with previous theoretical [51] and experimental findings [47]. At room temperature no red-shifted emission was observed, neither in solution nor in solid film. Since we did not observe any concentration dependence of the red-shifted emission we exclude aggregates, excimers or charge-transfer states as the source of this emission.

It is also apparent that the energy of the triplet state is rather independent of the details of the molecular structure, due to its stronger localization in comparison with the singlet state [21,22]. Thus, the reduction of the singlet–triplet gap is mainly due to the influence of the structure on the singlet state leading to a red-shift of the fluorescence of **A-DATP** and **L-DATP** compared with **TPTP** (Fig. 6). A similar conclusion was drawn from the experiments on triphenylene polymers [27].

3.3.1. OLEDs

To probe the favourable charge-transporting ability of triphenylenes [25] we investigated their performance in OLEDs. Keeping in mind the decent performance as fluorescence emitter [26], we used Ir(III) dyes as emitter for phosphorescent OLEDs. Since the T_1 energy of **TPTP**, **L-DATP** and **A-DATP** is comparable to the triplet state of green emitting Ir(III) dyes, we tested the triphenylenes as matrix for $Ir(mppy)_3$ ($T_1 \sim 2.4$ eV; 520 nm) doped, solution-processed OLEDs.

The best results were obtained with **TPTP** as matrix. Thus we elaborate on optimization steps in a little more detail. Besides variation of emitter concentration we introduced various functional layers such as electron transport layer (ETL), hole/exciton blocking layer and hole injection layers.

In a first set of experiments single-layer devices of **TPTP** (Scheme 2, device type **A**) with varying dopant concentration were fabricated and characterized. The current efficiency (emitted photons per injected electrons) increases from 2.5, 4.9 to 11.3 cd/A with dopant concentration increasing from 2.5%, 5% to 10% by mole, respectively. Correspondingly, the achievable brightness increases from 3000 cd/m^2 to more than 10.000 cd/m^2. The higher brightness with increasing $Ir(mppy)_3$ content (see Table 4) is attributed to better charge injection, transport and

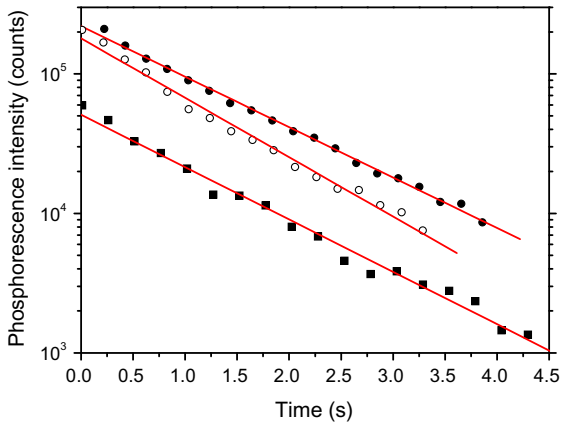

Fig. 4. Time dependence of phosphorescence intensity of **TPTP** in cyclohexane ($c = 5.6 \times 10^{-5}$ mol/L, squares), **L-DATP** in cyclohexane ($c \sim 1 \times 10^{-5}$ mol/L, solid circles) and **L-DATP** in DCM ($c = 2.3 \times 10^{-5}$ mol/L, open circles) vs time. The straight lines are fits to the data yielding phosphorescence lifetimes of 1.19 s (L-DATP/cyclohexane), 1.06 s (L-DATP/DCM) and 1.16 s (TPTP/cyclohexane), respectively. All measurements were done at 80 K.

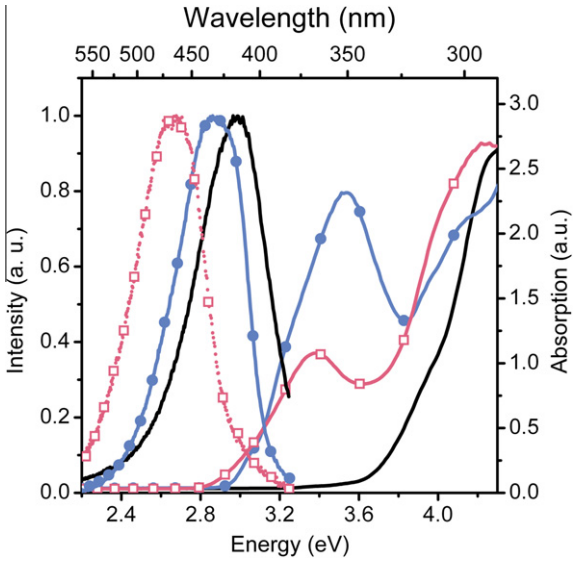

Fig. 5. Left axis: Fluorescence spectra of thin films of **TPTP** (solid line), **L-DATP** (dotted red line, squares) and **A-DATP** (dashed blue line dots). Right axis: Absorption spectra of thin films of **TPTP** (solid line), **L-DATP** (solid red line, squares) and **A-DATP** (solid blue line dots). (For interpretation of the references to colour in this figure legend, the reader is referred to the web version of this article.)

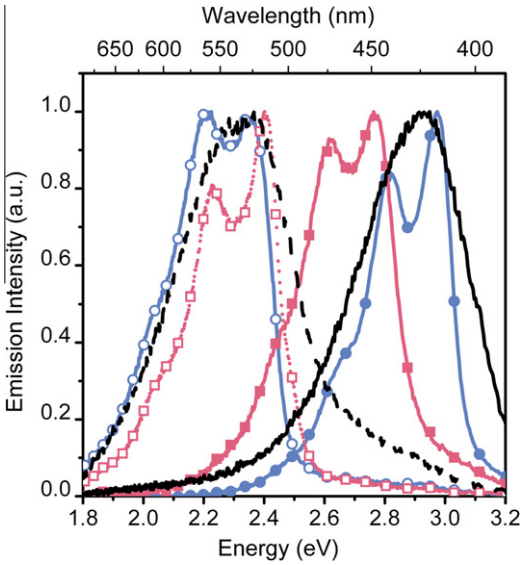

Fig. 6. Emission spectra corresponding to fluorescence (high energy part) and phosphorescence (low energy part) of thin films of **TPTP** (solid line and dotted line), **L-DATP** (solid red line with solid squares and dotted red line with open squares) and **A-DATP** (solid blue line with solid circles and dashed blue line with open circles). Measurements were carried out at 80 K. (For interpretation of the references to colour in this figure legend, the reader is referred to the web version of this article.)

recombination, simply, by considering that more transport/recombination sites are available. $Ir(mppy)_3$ has a smaller HOMO–LUMO gap compared with **TPTP** (Scheme 2). Similar observations were reported many times in other systems [14,16,17].

3.3.2. Electron transport layer

To optimize the device performance an electron transport layer, functioning as hole/exciton blocking layer simultaneously, on top of the emission layer was introduced. We chose a 20 nm thick TPBi layer due to its known blocking properties [9,52]. HOMO and LUMO levels of TPBi are located at −6.4 and −2.7 eV (Scheme 2b) [53]. The device architecture is depicted in Scheme 2a. In **TPTP**:$Ir(mppy)_3$ OLEDs the current efficiency increases significantly to 16.7, 30.5 to 31.3 cd/A with increasing dopant concentration from 2.5%, 5% to 10% by mole, respectively (Table 4, Fig. 7). This is a two to eight fold increase depending on concentration. Since TPBi blocks holes and excitons from reaching the cathode a shift of the emission zone closer to the anode side results. This is further substantiated by the enhanced emission of electroluminescence in the low energy part of the emission spectrum (see Fig. 8) in devices containing TPBi. Comparing device configuration **A** and **B**, the low energy emission is enhanced for the TPBi containing device **B**. The higher efficiency is, therefore, due to a better charge balance, leading to a confinement of the emission zone, thus improving recombination and optical out-coupling [54–56].

3.4. Hole injection layer

A further improvement of the efficiency might be possible by increasing the hole density in the device. From the energy levels (Scheme 2) it is apparent that there is a large energy barrier of 1.2 eV between the hole-injecting contact PEDOT:PSS (5.1 eV) and the **TPTP** HOMO level (6.3 eV). The HOMO energy of **TPTP** is calculated from the first oxidation potential at 1.18 V (assuming the validity of Koopman's theorem) using 5.1 eV as offset factor [44]. It can be expected, that the hole injection is limited in device type **A** and **B**. This is supported by the observation of increased efficiency and brightness upon increasing the amount of $Ir(mppy)_3$ loading, taking into account the favourable HOMO level of $Ir(mppy)_3$ at −5.3 eV [16].

To promote hole injection into **TPTP** we used crosslinkable hole-transport layers which were shown to improve device performance in numerous OLEDs [16–18]. Apparently, with **TPTP** this works as well, as the maximum performance of 30.8 cd/A is already obtained at 5% $Ir(mppy)_3$ loading (Table 4 and Fig. 7). However, the efficiency could not be raised above 31 cd/A. The lower efficiency at comparable voltage for devices **B** and **C** is partly due to a 20% larger thickness of device **C**. This can in principle be avoided, but is not of primary concern in the present work. The EL spectrum of device **C** is largely identical to device **B** (Fig. 8) pointing to a similar location of the recombination zones and similar out-coupling efficiency.

3.5. Adjusting electron density

Following the above discussion it is clear, that a limited hole density in the device cannot be the reason for the limited efficiency. Another source for improvement might be an increase in electron density to balance the hole density. The reduction potential of **TPTP** could not be obtained by cyclic voltammetry. It can be estimated from the HOMO

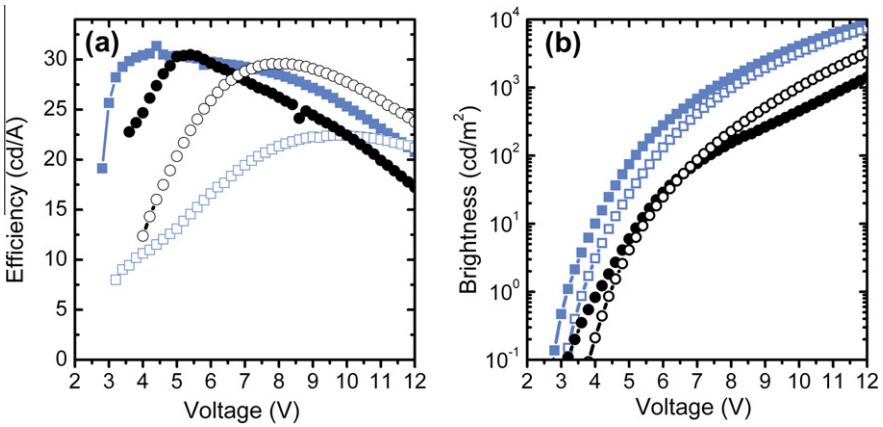

Fig. 7. Panel (a): Current efficiency of 5% (black) and 10% (blue) Ir(mppy)$_3$ doped **TPTP** OLEDs. Solid symbols refer to device type **B** and open symbols to device type **C**. Panel (b): The brightness of devices shown in (a) containing 5% (black) and 10% (blue) Ir(mppy)$_3$. Solid symbols refer to device type **B** and open symbols to device type **C**. (For interpretation of the references to colour in this figure legend, the reader is referred to the web version of this article.)

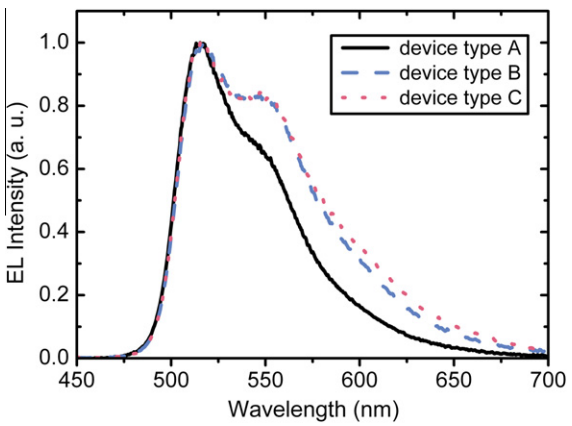

Fig. 8. Electroluminescence spectra of a **TPTP** OLED containing 10% Ir(mppy)$_3$.The emission spectra refer to devices of type **A** (black line), **B** (dashed blue line) and **C** (red dotted line). (For interpretation of the references to colour in this figure legend, the reader is referred to the web version of this article.)

level, the optical gap, and the exciton binding energy. In conventional organic semiconductors the exciton binding energy amounts to 0.5–0.7 eV [2]. Using this value we calculate the LUMO level to be located roughly at −2.8 to −2.6 eV in agreement with estimations for similar compounds [26]. Adopting a previously successful strategy [14–16] to improve electron transport in the bulk (i.e. matrix), we admixed the electron transporting material OXD-7 (25% by weight) to the **TPTP** matrix. The obtained maximum efficiency of device type **A** is 8.7 cd/A (Table 4) which is below the corresponding device without OXD-7 (11.3 cd/A, Table 4). Thus, electron transport in the bulk does not limit the device performance as can be expected from similar mobilities of electrons and holes in pure aromatic hydrocarbons [57].

Finally, the fact that the triplet energy of **TPTP** (2.37 eV, Table 3) and Ir(mppy)$_3$ (2.4 eV) are comparable, might open a significant loss channel by triplet back-transfer to the matrix. Thus, we tested the red-emitting Ir(t-piq)$_2$(acac) with a triplet energy of 1.98 eV (625 nm) for comparison. However, the efficiency decreased to 3 cd/A (Table 4). This is much lower than expected, even taking into account

Table 1
Calculated singlet transition energies, oscillator strength and singlet–triplet energy gap of the investigated compounds. The row composition gives the percentage to what extent one electron excitations (CI description) contribute to the total energy. Only transitions with a contribution of more than 5% are listed in the table.

Compound	**TPTP**	**L-DATP**	**A-DATP**
Absorption, $S_1 \leftarrow S_0$, [nm], [eV] (*fosc*)	335, 3.70 (0.002)	419, 2.96 (0.143)	408, 3.04 (0.095)
Composition of S_1 [%]	HOMO→LUMO + 1	HOMO → LUMO	HOMO → LUMO
	54 HOMO-1 → LUMO	88 HOMO → LUMO + 1	77 HOMO-1 → LUMO + 1
	42	7	16
Absorption, $S_2 \leftarrow S_0$, [nm], [eV] (*fosc*)	323, 3.84 (0.079)	411, 3.02 (0.110)	395, 3.14 (0.211)
Composition of S_2 (%)	HOMO → LUMO	HOMO → LUMO + 1	HOMO → LUMO + 1
	84 HOMO-1 → LUMO + 1	85 HOMO → LUMO	75 HOMO-1 → LUMO
	13	8	22
Composition of T_1 (%)	HOMO → LUMO	HOMO → LUMO	HOMO → LUMO + 1
	61 HOMO-1 → LUMO + 1	62 HOMO → LUMO + 2	52 HOMO-1 → LUMO 25
	19 HOMO-2 → LUMO + 2	16	HOMO-2 → LUMO
	7		6
Calculated singlettriplet splitting (S_1–T_1) ΔE_{ST} (eV)	0.75	0.35	0.47

Table 2
Optical properties of **TPTP** and **L-DATP** measured in dichloromethane (DCM) and cyclohexane solution. Absorption and fluorescence (PL) data are taken at room temperature, whereas phosphorescence (Phos) was measured at 80 K.

Compound/solvent	Absorption edge (nm), (eV)	Absorption[a] (nm), (eV)	Absorption (max.) (nm), (eV)	PL (max.) (nm), (eV)	Phos (max.) (nm), (eV)	Phos lifetime (s)
TPTP/DCM	~363, 3.42	314, 3.95	288, 4.3	396, 3.13	~545, 2.27	1.2
TPTP/cyclo-hexane		314, 3.95	289, 4.28	396, 3.13	~535, 2.3	1.16
L-DATP/DCM	~436, 2.84	364, 3.41	292, 4.24	479, 2.59	527, 2.35	1.06
L-DATP/cyclo-hexane		365, 3.4	292, 4.24	451, 2.75	521, 2.38	1.19

[a] For TPTP this corresponds to the low energy shoulder of the main absorption band and for L-DATP it is the maximum of the low energy band.

Table 3
Optical properties of **TPTP**, **L-DATP** and **A-DATP** measured in thin films. Absorption, fluorescence (PL) and fluorescence quantum yield (PLQY) data refer to room temperature data if not stated otherwise, whereas phosphorescence (Phos) was measured at 80 K.

Compound (film)	TPTP	L-DATP	A-DATP
Absorption edge, $S_1 \leftarrow S_0$ (nm), (eV)	330, 3.75	430, 2.88	421, 295
Absorption[a] (nm), (eV)	315, 3.94	416, 2.98	404, 3.07
Absorption Maximum[b] (nm), (eV)	290, 4.28	368, 3.37	351, 3.53
PL[c] S_0–S_1 (nm), (eV)	400 (3.1)	448 (2.76)	417 (2.97)
PLQY	0.15	0.2	0.16
PL lifetime (ns)	–	5.15	5.05
Phos[c], S_0–T_1 (nm), (eV)	523 (2.37)	516 (2.4)	527 (2.35)
Calculated singlet–triplet splitting (S_1-T_1) ΔE_{st} [eV]	0.75	0.35	0.47
Measured singlet–triplet splitting[c] (S_1–T_1) ΔE_{st} (eV)	0.73	0.36	0.62

[a] shoulder on the low energy tail of absorption.
[b] maximum of the low energy band for L-DATP and A-DATP (see Fig. 5).
[c] derived from 80 K spectra (Fig. 6), see text for details.

the lower phosphorescence yield of Ir(t-piq)$_2$(acac) compared with Ir(mppy)$_3$. With Ir(t-piq)$_2$(acac) as emitter roughly 18 cd/A should be achievable [52]. Thus, triplet transfer from the Ir(III)-complex to **TPTP** cannot be the only reason for the observed loss in efficiency. Since the triplet diffusion length is in the range of tens of nanometers, triplets might get lost by transfer to the adjacent HTL and ETL. TPBI has a triplet energy of 2.6 eV [58] and losses are not expected to be dominant. More important in this respect is the relatively low triplet energy of around 2.3 eV of the HTL [59], suggesting that a large part of the losses are due to triplet transfer to the HTL followed by non-radiative recombination.

Recent results from the literature [60], where high efficiency in a phosphorescent OLED has been obtained with a matrix having a lower triplet level than the Ir(III)-emitter, and the reduced performance of the **TPTP**:Ir(t-piq)$_2$(acac) devices hint that there might be additional loss channels. At present we can only speculate about the cause. It is known from investigations on vacuum-deposited Ir(III) dye doped devices that aggregation of the dyes takes place even at low (1%) dopant concentration [61]. Although we cannot prove that this happens in our devices, it is highly probable considering the different molecular shape of the dopant and matrix materials. It is apparent from Fig. 7 that already at a moderate brightness of a few hundred cd/m^2, the efficiency decreases. We attribute this decrease to triplet–triplet annihilation (TTA), possibly enhanced by aggregation of the dopant. Besides triplet back-transfer this might account for the limited efficiency of the devices.

3.6. L-DATP and A-DATP OLEDs

The efficiency of the **L-DATP** and **A-DATP** OLEDs type **A** with Ir(mppy)$_3$ as emitter remains below 1 cd/A even at higher (20%) dopant concentration. This can be rationalized by having a close look at the energy levels (Scheme 2). The HOMO energies of both compounds were calculated according to the procedure used for **TPTP** (see above). From the oxidation potentials of **L-DATP** (0.2 V) and **A-DATP** (0.4 V) a HOMO energy of 5.3 and 5.5 eV, respectively, can be estimated. Thus, we expect the current is dominated by holes in both materials. Since the HOMO is comparable to that of Ir(mppy)$_3$, holes have a low probability of recombination due to the lack of trapping at Ir(mppy)$_3$ before being discharged, even at 20% Ir(mppy)$_3$ loading. This is substantiated by the observation of residual electroluminescence in the 400–480 nm region

Table 4
Efficiency data of Ir(mppy)3 doped **TPTP** OLEDs of varying dopant concentration, architecture and composition. **A**, **B** and **C** in column one refer to devices architectures in Scheme 2.

Compound, Ir(mppy)3 conc., device type	Max. luminous efficiency (cd/A)	Max. power efficiency (lm/W)	Performance @ 100 cd/m^2 (cd/A)	Performance @ 1000 cd/m^2 (cd/A)
TPTP, 2.5 **A**; **B**	2.5; 16.7	0.8; 6.9	0.2; 11.7	1.6; –
TPTP, 5 **A**; **B**	4.9; 30.5	1.7; 17.7	0.6; 27.1	3.5; 18.9
TPTP, 10 **A**; **B**	11.3; 31.3	4.2; 22.4	1.7; 30.3	7; 28.8
TPTP, 5 **C**	30.8	12.7	30.6	28.2
TPTP, 10 **C**	22.3	7.8	15.9	21.6
TPTP, 10 OXD-7 **A**	8.7	1.6	6.3	–
TPTP 10 Ir(t-piq)$_2$(acac) **A**	2.9	1.8	2.5	–

(not shown) being due to recombination in the **L-DATP** and **A-DATP** matrix.

Though the introduction of a hole/exciton blocking layer of TPBi (device type **B**) increased the efficiency, it remained below 5 cd/A in all cases. This points to a rather high hole density, making it difficult to achieve charge balance at all, hence no further optimization was carried out.

4. Summary

We have shown that substitution is an effective tool to control the energy splitting of singlet and triplet excitons in conjugated organic macromolecules. The singlet–triplet gap in a tetraphenyl-substituted triphenylene **TPTP** is reduced from ~0.8 to 0.3 eV upon substitution with diphenylamine groups. Theoretical predictions on the variation of the energy gap were verified by fluorescence and phosphorescence spectroscopy. Application of the triphenylenes as matrix materials in $Ir(mppy)_3$-doped OLEDs revealed good device performance for **TPTP**. It was shown that the efficiency is not limited by intrinsic materials properties such as injection or transport of charge. At present we can only speculate that losses are due to a combination of triplet back-transfer from the Ir(III)-dye to the matrix followed by non-radiative recombination and triplet–triplet and triplet-charge annihilation induced by limited intermixing of the materials constituting the blend. However, the ability to tune the singlet–triplet gap might be very useful for device application such as solar cells of the next generation, where singlet fission into triplets might be used to increase the current generation efficiency [31].

Acknowledgement

We would like to thank DFG for financial support via HE 5577/1 (D.H.) and SFB 813 (S.H. and F. N.).

References

[1] B.K. Yap, R.D. Xia, M. Campoy-Quiles, P.N. Stavrinou, D.D.C. Bradley, Nat. Mater. 7 (2008) 376.
[2] D. Hertel, H. Bässler, Chem. Phys. Chem. 9 (2008) 666.
[3] Special issue organic electronics and optoelectronics, Chem. Rev. 107 (2007) 923.
[4] D. Braga, G. Horowitz, Adv. Mater. 21 (2009) 1473.
[5] P. Zacharias, M.C. Gather, A. Köhnen, N. Rehmann, K. Meerholz, Angew. Chem., Int. Ed. 48 (2009) 4038.
[6] G. Dennler, M.C. Scharber, Ch.J. Brabec, Adv. Mater 21 (2009) 1323.
[7] M.A. Baldo, D.F. O'Brien, Y. You, A. Shoustikov, S. Sibley, M.E. Thompson, S.R. Forrest, Nature 395 (1998) 151.
[8] M.A. Baldo, M.E. Thompson, S.R. Forrest, Nature 403 (2000) 750.
[9] K. Walzer, B. Maennig, M. Pfeiffer, K. Leo, Chem. Rev. 107 (2007) 1233.
[10] S. Reineke, F. Lindner, G. Schwartz, N. Seidler, K. Walzer, B. Luessem, K. Leo, Nature (2009) 459 234.
[11] S.R. Forrest, Nature 428 (2004) 911.
[12] H. Sasabe, J. Takamatsu, T. Motoyama, S. Watanabe, G. Wagenblast, N. Langer, O. Molt, E. Fuchs, C. Lennartz, J. Kido, Adv. Mater. 22 (2010) 5003.
[13] D.C. Müller, A. Falcou, N. Reckefuss, M. Rojahn, V. Wiederhirn, P. Rudati, H. Frohne, O. Nuyken, H. Becker, K. Meerholz, Nature 421 (2003) 829.
[14] X.H. Yang, T. Däubler, D. Hertel, D. Neher, Adv. Mater. 16 (2004) 161.
[15] M.K. Mathai, V.E. Choong, S.A. Choulis, B. Krummacher, F. So, Appl. Phys. Lett. 88 (2006) 243512.
[16] X.H. Yang, D.C. Müller, D. Neher, K. Meerholz, Adv. Mater. 18 (2006) 948.
[17] N. Rehmann, D. Hertel, H. Becker, S. Heun, K. Meerholz, Appl. Phys. Lett. 91 (2007) 103507.
[18] N. Rehmann, C. Ulbricht, A. Köhnen, P. Zacharias, M.C. Gather, D. Hertel, E. Holder, K. Meerholz, U.S. Schubert, Adv. Mater. 20 (2008) 129.
[19] A. van Dijken, J.J.A.M. Bastiaansen, N.M.M. Kiggen, B.M.W. Langeveld, C. Rothe, A. Monkman, I. Bach, P. Stossel, K. Brunner, J. Am. Chem. Soc. 123 (2004) 7718.
[20] M.A. Baldo, C. Adachi, S.R. Forrest, Phys. Rev. B 62 (2000) 10967.
[21] D. Hertel, S. Setayesh, H.G. Nothofer, U. Scherf, K. Müllen, H. Bässler, Adv. Mat. 13 (2001) 65.
[22] A. Köhler, D. Beljonne, Adv. Funct. Mater. 14 (2004) 11.
[23] L.S. Devi, M.K. Al-Suti, C. Dosche, M.S. Khan, R.H. Friend, A. Köhler, Phys. Rev. B 78 (2008) 045210.
[24] D. Adam, P. Schuhmacher, J. Simmerer, L. Häussling, K. Siemensmeyer, K.H. Etzbach, H. Ringsdorf, D. Haarer, Nature 371 (1994) 141.
[25] X.L. Feng, V. Marcon, W. Pisula, M.R. Hansen, J. Kirkpatrick, F. Grozema, D. Andrienko, K. Kremer, K. Müllen, Nat. Mater. 8 (2009) 421.
[26] H. Wettach, S. Jester, A. Colsmann, U. Lemmer, N. Rehmann, K. Meerholz, S. Höger, Synth. Met. 160 (2010) 691.
[27] D. Chaudhuri, H. Wettach, K.J. van Schooten, S. Liu, E. Sigmund, S. Höger, J.M. Lupton, Angew. Chem. 49 (2010) 7741.
[28] V.A. Dediu, L.E. Hueso, I. Bergenti, C. Taliani, Nat. Mater. 8 (2009) 707.
[29] T.D. Nguyen, G. Hukic-Markosian, F. Wang, L. Wojcik, X.-G. Li, E. Ehrenfreund, Z.V. Vardeny, Nat. Mater. 9 (2010) 345.
[30] J.M. Lupton, D.R. McCamey, C. Boehme, Chem. Phys. Chem. 11 (2010) 3040.
[31] A. Rao, M.W.B. Wilson, J.M. Hodgkiss, S. Albert-Seifried, H. Bässler, R.H. Friend, J. Am. Chem. Soc. 132 (2010) 12698.
[32] W. Dilthey, S. Henkels, A. Schaefer, Chem. Ber. 71B (1938) 974.
[33] R.A. Pascal Jr., D. Van Engen, B. Kahr, W.D. McMillan, J. Org. Chem. 53 (1988) 1687.
[34] J.W. Ciszek, J.M. Tour, Tet. Lett. 45 (2004) 2801.
[35] R. Callahan, K. Marshall, R. Rothchild, K. Rosmarion, Chem. Educator 6 (2001) 227.
[36] A.D. Becke, Phys. Rev. A. 38 (1988) 3098.
[37] J.P. Perdew, Phys. Rev. B 33 (1986) 8822.
[38] A. Schäfer, H. Horn, R. Ahlrichs, J. Chem. Phys. 97 (1992) 2571.
[39] S. Grimme, J. Comp. Chem. 27 (2006) 1787.
[40] F. Neese, G. Olbrich, Chem. Phys. Lett. 362 (2002) 170.
[41] A. Dreuw, M. Head-Gordon, Chem. Rev. 105 (2005) 4009.
[42] F.J. Devlin, P.J. Stephens, J.R. Cheeseman, M.J. Frisch, J. Am. Chem. Soc. 118 (1996) 6327.
[43] D. Hertel, K. Meerholz, J. Phys. Chem. B. 111 (2007) 12075.
[44] Zacharias, P. Gather, M. C. Rojahn, M. Nuyken, O. Meerholz, K. Angew. Chem., Int. Ed. 46 (2007) 4388.
[45] J. Gierschner, J. Cornil, H.-J. Egelhaaf, Adv. Mater. 19 (2007) 173.
[46] C. Reichardt, Chem. Rev. 94 (1994) 2319.
[47] D. Hertel, S. Setayesh, H.-G. Nothofer, U. Scherf, K. Müllen, H. Bässler, et al., Adv. Mat. 13 (2001) 65.
[48] R. Sasson, O. Braitbart, A. Weinreb, J. Lumin. 39 (1988) 223.
[49] G. Heimel, M. Daghofer, J. Gierschner, E.J.W. List, A.C. Grimsdale, K. Müllen, D. Beljonne, J.L. Brédas, E. Zojer, J. Chem. Phys. 122 (2005) 054501.
[50] Errors introduced upon estimation of transition energies from experimental spectra using different spectral features has been discussed in some detail in ref. [45].
[51] A. Köhler, D. Beljonne, Adv. Funct. Mater. 11 (2004) 14.
[52] N. Tian, A. Thiessen, R. Schiewek, O.J. Schmitz, D. Hertel, K. Meerholz, E. Holder, J. Org. Chem. 74 (2009) 2718.
[53] R. Pode, S.-J. Lee, S.-H. Jin, S. Kim, J.H. Kwon, Phys. D: Appl. Phys. 43 (2010) 25101.
[54] S.L.M. van Mensfoort, M. Carvelli, M. Megens, D. Wehenkel, M. Bartyzel, H. Greiner, R.A.J. Janssen, R. Coehoorn, Nat. Photon. 4 (2010) 329.
[55] S. Harkema, R.A.H.J. Kicken, B.M.W. Langeveld-Voss, S.L.M. van Mensfoort, M.M. de Kok, R. Coehoorn, Org. Electron. 11 (2010) 755.
[56] M.C. Gather, M. Flammich, N. Danz, D. Michaelis, K. Meerholz, Appl. Phys. Lett. 94 (2009) 263301.
[57] M. Pope, C.E. Swenberg, Electronic Processes in Organic Crystals and Polymers, Oxford University Press, New York, 1999.

[58] H. Fukugawa, K. Watanabe, S. Tokito, Org. Electron. 10 (2009) 798.
[59] C. Ulbricht, N. Rehmann, E. Holder, D. Hertel, K. Meerholz, U.S. Schubert, Macromol. Chem. Phys. 210 (2009) 531.
[60] J.S. Swensen, E. Polikarpov, A. von Ruden, L. Wang, S. Linda, A. Sapochak, B. Padmaperuma, Adv. Funct. Mater. 21 (2011) 3250.
[61] S. Reineke, G. Schwartz, K. Walzer, M. Falke, K. Leo, Appl. Phys. Lett. 94 (2009) 163305.